Defect Engineering of Air-stable Li_5FeO_4 towards Ultra-high Capacity Cathode Prelithiation Additive

*Bin Zhu[a], Naifeng Wen[a], Jingyang Wang[b,] *, Qiyu Wang[a], Jingqiang Zheng[a], Zhian Zhang[a,] **

[a]School of Metallurgy and Environment, National Energy Metal Resources and New Materials Key Laboratory, Central South University, Changsha 410083, People's Republic of China

[b]School of Sustainable Energy and Resources, Nanjing University, Suzhou, 215163, China；

corresponding author E-mail: zhangzhian@csu.edu.cn; jy_wang@nju.edu.cn

1. Experimental

1.1. Material synthesis

The LFO synthesis method has been reported in a previous article[1, 2]. To synthesize LFO-Zr, a certain amount (1%, 3% and 5% by mol) of Zirconium source ($Zr(OC_2H_5)_4$, Aladdin, 97.0%) and LFO powder was mixed up well in tetrahydrofuran (THF) for 8 h. Then the powder was taken out to be dried and calcinated at 700 ℃ in Ar. Finally, the LFO-Zr prelithiation material was obtained after being cooled down to room temperature.

1.2. Electrochemical characterizations

Active material, super P and polyvinylidene fluoride (PVDF) binder were evenly mixed in N-methylpyrrolidone solvent at a ratio of 7:2:1 and then coated on the surface of the aluminum foil. The positive electrode plate was cut into a 10 mm diameter pole plate, and the lithium anode electrode and graphite anode electrode are assembled into half-cell and full-cell, respectively. The charge and discharge test and Galvanostatic Intermittent Titration Technique (GITT) were tested on the LANDCT-2001A battery tester[3, 4]. Cyclic voltammetry (CV, 0.1mV s^{-1}) and *in-situ* electrochemical impedance spectroscopy (EIS, 0.1~100000 Hz) were performed using an electrochemical workstation (Gamry, Reference 600).

1.3. Materials characterizations

The phase composition was measured by X-ray diffraction (XRD, Cu Kα radiation, Rigaku MiniFlex 600) at a scan rate of 10° min^{-1}. Scanning electron microscopy of Navi

New Materials (SEM, TESCAN company) and transmission electron microscopy (TEM, Tecnai G2 F20) were used to observe the microstructure of materials. Electronic signals and valence state information at different depths were tested by an Ar^+ etched X-ray photoelectronic spectrometer of Shiyanjia Lab (www.shiyanjia.com). The sulfur carbon analyzer was applied to test the carbon content. Fourier Transform Infrared (FT-IR) Spectroscopy was used to detect functional groups in the products of materials after exposure to air. Differential electrochemical mass spectrometry (DEMS, Shanghai Zerolu Instrument Co.) is employed to analyze gas generation during charge/discharge.

1.4 DFT Calculation

All calculations in this study were performed with DFT using the VASP package. Projector augmented-wave potentials with a kinetic energy cutoff of 520 eV and the exchange-correlation form in the Perdew–Burke–Ernzerhof generalized gradient approximation (GGA-PBE) were employed with spin polarization and rotationally invariant scheme of Hubbard-U correction[5]. The values of Ueff = 5.3 was employed for Fe[6]. Structures with Li/vacancy orderings were prescreened using an electrostatic energy criterion followed by DFT geometry optimizations[7]. For all the calculations, at least 1200 k-points per reciprocal atom was applied, and the convergence criteria were set as 10−5 eV for electronic iterations and 0.03 eV/Å for ionic iterations[8]. Gaussian smearing with a width of 0.05 eV was implemented to enhance the convergence of electronic minimization. DFT-D3 method was utilized to incorporate van der Waals interaction[9]. NEB calculations were performed in DFT with the initial and final Li-ion configurations shown in Figure 1.

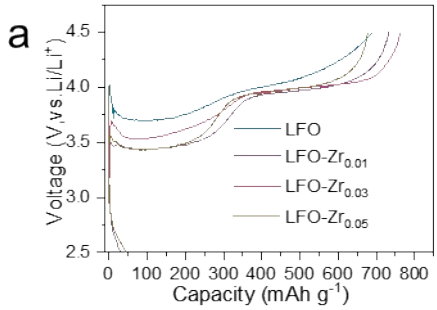

Figure S1. The initial charge/discharge profiles of LFO cathode with different Zr content and without Zr.

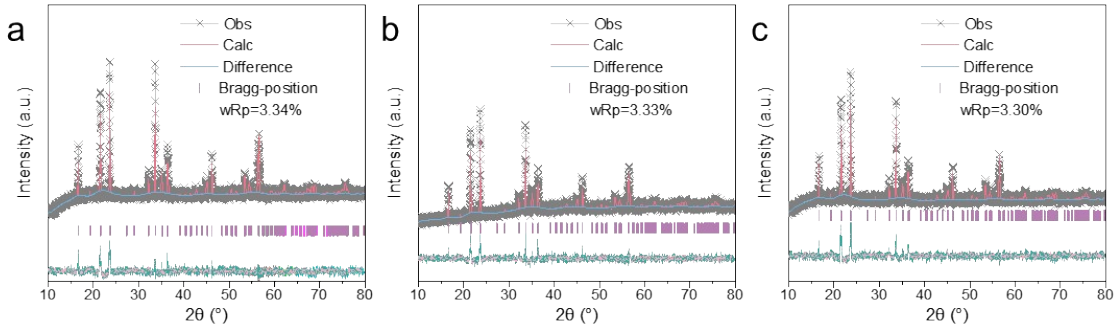

Figure S2. The Rietveld XRD pattern of LFO (a), LFO-$Zr_{0.01}$(b) and LFO-$Zr_{0.05}$(c).

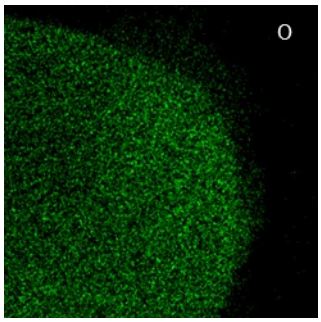

Figure S3. EDS mapping of LFO-$Zr_{0.03}$

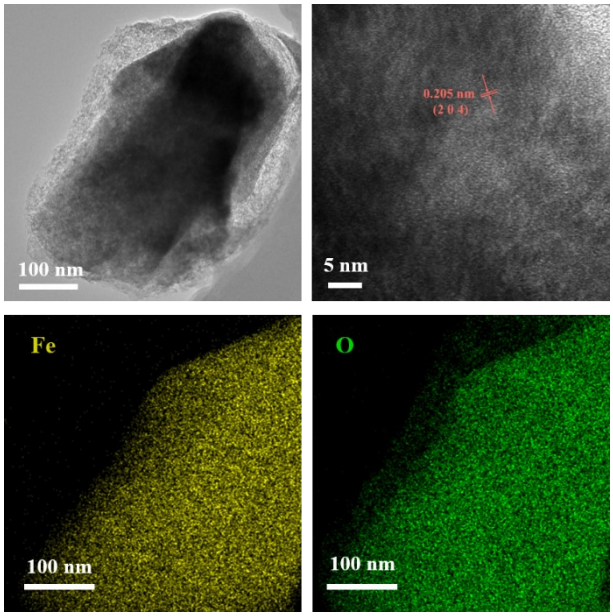

Figure S4. TEM image and HRTEM image and EDS mapping of LFO.

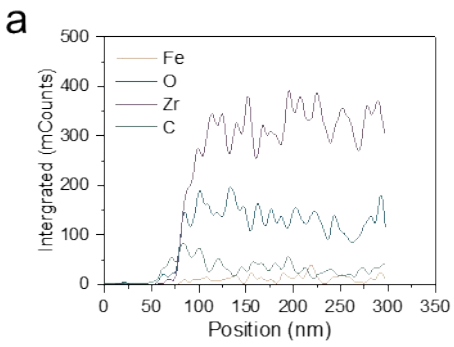

Figure S5. The line sweep image of LFO-$Zr_{0.03}$.

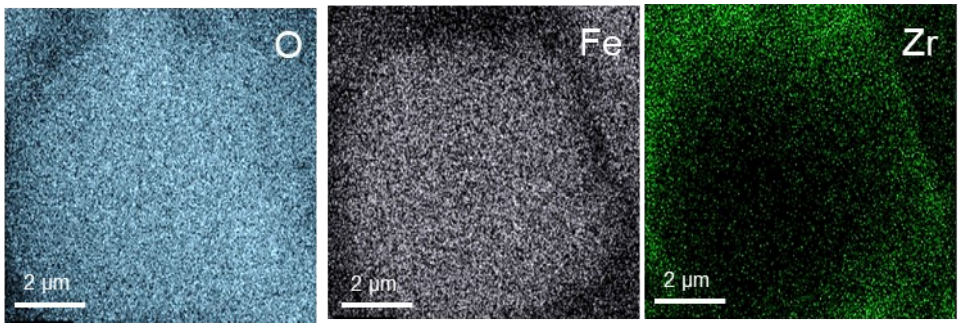

Figure S6. The FIB-SEM mapping images of LFO-$Zr_{0.03}$.

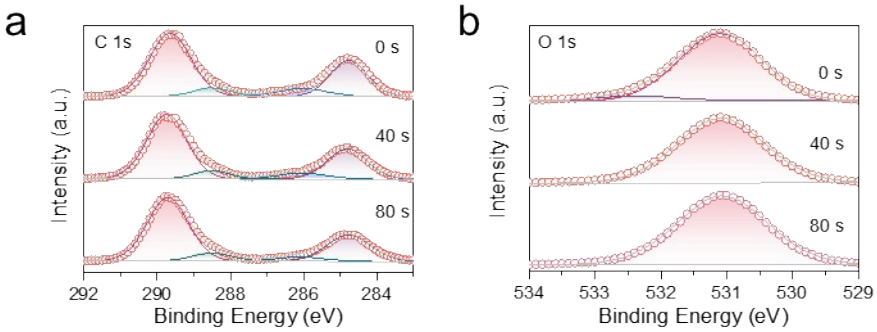

Figure S7. C 1s (a) and O 1s of etch LFO-$Zr_{0.03}$ at 0, 40, 80 s.

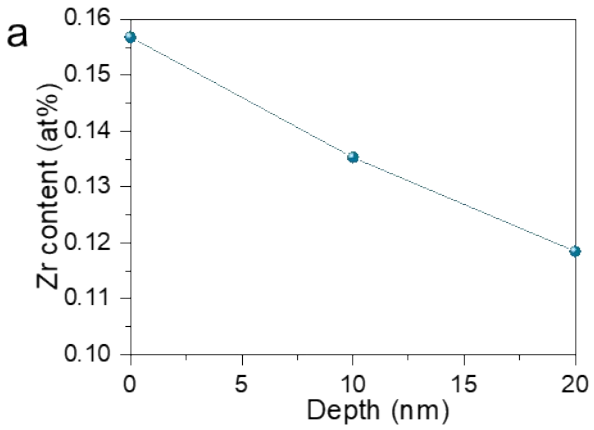

Figure S8. Zr content at different etching depths

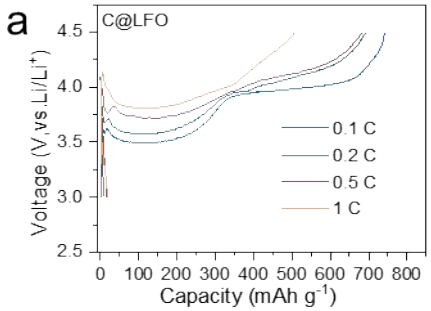

Figure S9. Initial charge/discharge curves at different rates of C@LFO.

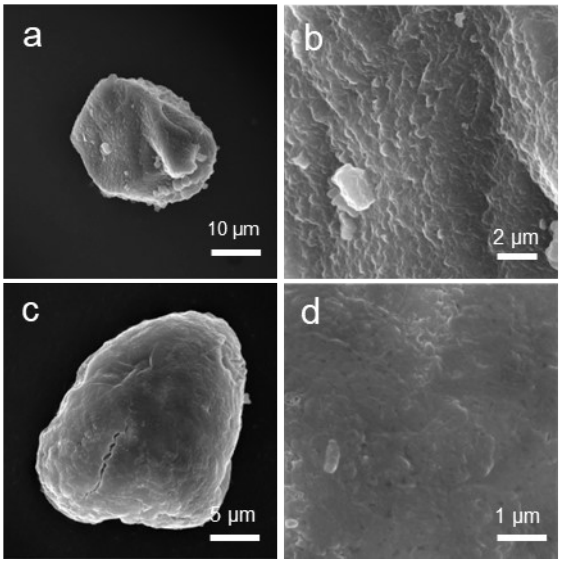

Figure S10. The SEM images of LFO and LFO-$Zr_{0.03}$ exposed in 20% humidity air for 8h.

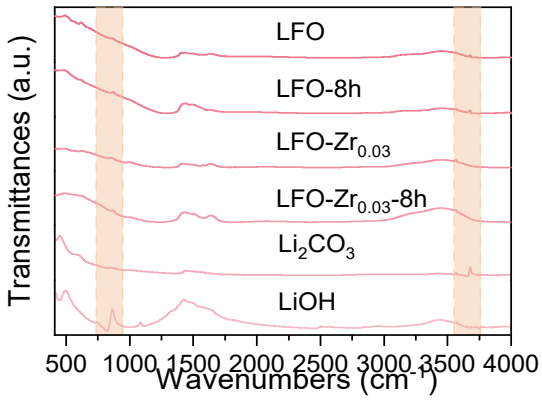

Figure S11. FT-IR spectrum of LFO, LFO-$Zr_{0.03}$ and their post-exposure products.

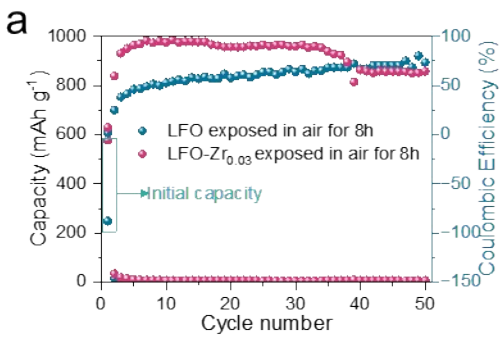

Figure S12. Cycle performance of LFO and LFO-$Zr_{0.03}$ at 0.1C after exposed in 20% humidity air.

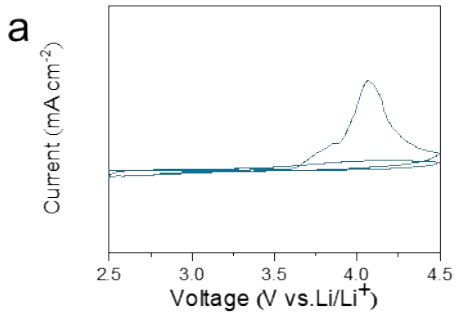

Figure S13. CV of LFO-$Zr_{0.03}$ at 0.1mV s^{-1} after exposed in 20% humidity air.

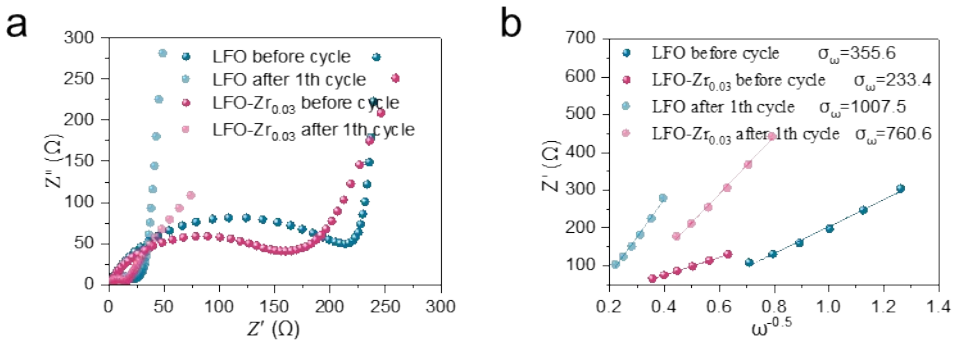

Figure S14. Impedance spectra (a) and Z'-$\omega^{-1/2}$ curves (b) of LFO and LFO-$Zr_{0.03}$ before and after cycle, respectively.

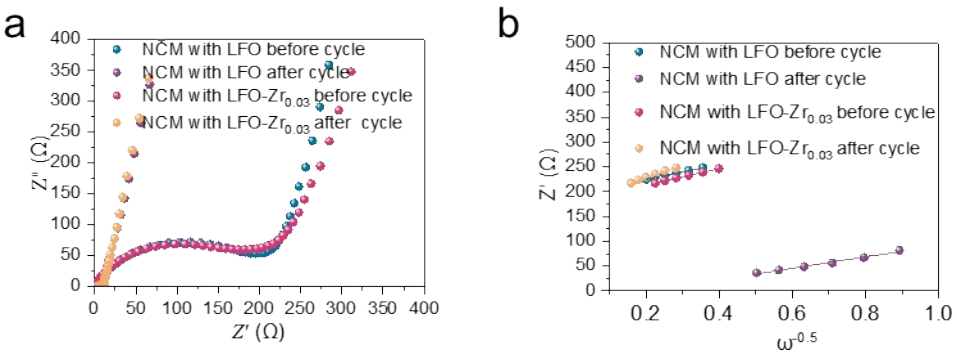

Figure S15. The EIS (d) and Z'-$\omega^{-0.5}$ (e) of NCM with LFO and LFO-$Zr_{0.03}$ electrode.

Table S1. Positron lifetime parameters of the pristine LFO and LFO-Zr

Date	Lifetime τ1	Intensity	Lifetime τ2	Intensity	Lifetime τ3	Intensity
LFO	0.095	21.4	0.192	77.9	1.579	0.658
LFO-Zr	0.127	39.1	0.224	60.2	1.538	0.780

Table S2. Calculated lattice parameters for pristine and Zr-doped Li_5FeO_4.

Composition	a (Å)	b (Å)	c (Å)	Volume
LFO	9.111	9.128	9.140	760.13
$Li_5Fe_{0.875}Zr_{0.125}O_4$	9.159	9.117	9.181	766.62

Table S3 The Rietveld XRD parameter of LFO, LFO-$Zr_{0.01}$, LFO-$Zr_{0.03}$ and LFO-$Zr_{0.05}$

	a (Å)	c (Å)	wRp (%)	Rp (%)
LFO	9.239406	9.168834	3.34	2.47
LFO-$Zr_{0.01}$	9.239712	9.168847	3.30	2.39
LFO-$Zr_{0.03}$	9.242759	9.173456	1.38	0.95
LFO-$Zr_{0.05}$	9.244131	9.174272	3.33	2.50

Table S4 Sulfur carbon analysis test results of LFO-$Zr_{0.01}$, LFO-$Zr_{0.03}$ and LFO-$Zr_{0.05}$

Sample	C (wt%)
LFO-$Zr_{0.01}$	0.54
LFO-$Zr_{0.03}$	0.99
LFO-$Zr_{0.05}$	1.43

Table S5. Comparison of the properties of different pre-lithiation reagents.

	Price ($ Kg^{-1})	Li compensation capacity (mol)	Air stability	Delithium electrochemical windows (V)	Rate performance	Ref.
Li_2NiO_2	3053	1.2	general	3.5-4.3	general	10 11
Li_6CoO_4	7229	6	well	3.3-4.5	well	12
Li_5FeO_4	1401	4	sensitive	3.5-4.5	poor	2
This work	2282	～4.4	general	3.4-4.5	general	

Note：Prices of raw materials refer to Aladdin

Reference

1. B. Zhu, W. Zhang, Q. Wang, Y. Lai, J. Zheng, N. Wen and Z. Zhang, *Advanced Functional Materials*, 2024, 2315010.
2. J. Li, B. Zhu, S. Li, D. Wang, W. Zhang, Y. Xie, J. Fang, B. Hong, Y. Lai and Z. Zhang, *Journal of The Electrochemical Society*, 2021, **168**, 080510.
3. B. H. Toby, *JOURNAL OF APPLIED CRYSTALLOGRAPHY*, 2001, **34**, 210-213.
4. S. C. Vogel, *Journal of Applied Crystallography*, 2011, **44**, 873-877.
5. G. Kresse and J. Furthmüller, *Physical Review B*, 1996, **54**, 11169-11186.
6. J. P. Perdew, K. Burke and M. Ernzerhof, *Physical Review Letters*, 1996, **77**, 3865-3868.
7. A. Jain, S. P. Ong, G. Hautier, W. Chen, W. D. Richards, S. Dacek, S. Cholia, D. Gunter, D. Skinner, G. Ceder and K. A. Persson, *APL Materials*, 2013, **1**.
8. S. P. Ong, W. D. Richards, A. Jain, G. Hautier, M. Kocher, S. Cholia, D. Gunter, V. L. Chevrier, K. A. Persson and G. Ceder, *Computational Materials Science*, 2013, **68**, 314-319.
9. S. Grimme, J. Antony, S. Ehrlich and H. Krieg, *The Journal of Chemical Physics*, 2010, **132**.
10. Y. Wu, W. Zhang, S. Li, N. Wen, J. Zheng, L. Zhang, Z. Zhang and Y. Lai, *ACS Sustainable Chemistry & Engineering*, 2023, **11**, 1044-1053.
11. M. G. Kim and J. Cho, *Journal of Materials Chemistry* 2008, **18**, 5880-5887.
12. W. Lee, H. Lee, Y. Byeon, J. H. Kim, W. Choi, M. Choi, M. S. Park and W. S. Yoon, *Advanced Energy Materials*, 2023, **13**, 2302316.